Section S1. Evaporation rate of compound X

The evaporation rate of a compound from an aerosol particle that has been used for modeling the FIGAERO thermograms is (Schobesberger et al., 2018):

$$\frac{dN_i}{dt} = -\frac{1}{\sqrt{2\pi \cdot k_B \cdot m_i \cdot T}} P^*_{i,0} \cdot \chi_i \cdot \alpha \cdot \Gamma(Kn) \cdot A \cdot \exp\left(-\frac{\Delta H}{R}\left(\frac{1}{T} - \frac{1}{T_0}\right)\right) \quad \text{(S1)}$$

N_i: number of molecules indexed i .

k_B: Boltzmanns constant.

m_i: molecular mass of compound i .

T : temperature.

T_0: room temperature.

$P^*_{i,0}$: vapor pressure at $T = T_0$.

χ_i: mass fraction of compound i .

α: evaporation coefficient.

$\Gamma(Kn)$: factor correcting for limitations due to diffusion.

A : surface area of interface between aerosol-phase and gas-phase.

ΔH : enthalpy of evaporation.

R : universal gas constant

To make a simple model, that can be applied compound by compound, the surface area is assumed to be constant, and the same is assumed for the mass fraction of a given compound to the bulk particle-phase mass concentration. These assumptions are not likely to be the real case but are necessary for the very simple model we are trying to achieve. The factor $\Gamma(Kn)$ is assumed to be always close to one. Then by grouping all the terms that are independent of temperature and time, along with constants for converting into units of mass concentration, into one constant C_1 we obtain:

$$\frac{d[X]_{particle}}{dt} = -\frac{C_{1,i}}{\sqrt{T}}[X]_{particle} \exp\left(-\frac{\Delta H}{R}\left(\frac{1}{T} - \frac{1}{T_0}\right)\right) \quad \text{(S2)}$$

$C_{1,i}$ can be expressed using another positive constant T^* as:

$$C_{1,i} = \sqrt{T^*} \cdot \exp\left(-\frac{\Delta H}{R}\left(\frac{1}{T_0} - \frac{1}{T^*}\right)\right) \cdot \frac{1}{s} \quad \text{(S3)}$$

By renaming $k = \frac{\Delta H}{R}$ we obtain the temperature dependence function used in this work (Equation 1). T^* was used as a parameter for fitting since it represents the temperature where the evaporation rate exceeds $[X]_{particle} \cdot \frac{1}{s}$. Equation S3 has a minimum at $T^* = \frac{2\Delta H}{R}$, since values of $C_{1,i}$ lower than this minimum yield evaporation rates that never exceed $[X]_{particle} \cdot \frac{1}{s}$. This did not prove to be a problem during fitting. T^* was also restricted to be less than $\frac{2\Delta H}{R}$during fitting, resulting in T^* values that are located close to the beginning of the upward slope of the thermograms. Note that $T^* > \frac{2\Delta H}{R}$ result in exactly the same fits, but with a less intuitive parameter value.

Section S2. Particle transmission efficiency within the vaporization tube

The setting velocity v_S is calculated using the following equations (Hinds, 1999):

$$v_S = \frac{\rho_p d^2 g C_C}{18u} \quad \text{(S4)}$$

$$C_C = 1 + \frac{\lambda}{d}[2.34 + 1.05\exp(-0.39\frac{d}{\lambda})] \quad \text{(S5)}$$

ρ_p: the density of NaCl particles, 2.16 g cm^{-3}

d: diameter of the particle

g: gravitational acceleration, 9.81 m·s^{-2}

C_C: slip (Cunningham) correction factor

u: dynamic (absolute) viscosity of air

λ: mean free path of air

The particle diffusion (Brownian motion) constant D and root mean square distance of diffusion Y is calculated using the following equations (Hinds, 1999):

$$D = \frac{kTC_C}{3\pi u d} \quad \text{(S5)}$$

$$Y = \sqrt{2\mathrm{Dt}} \quad \text{(S6)}$$

k: the Boltzmann constant, 1.38 × 10^{-23} N m K^{-1}

T: Temperature

t: particle travel time

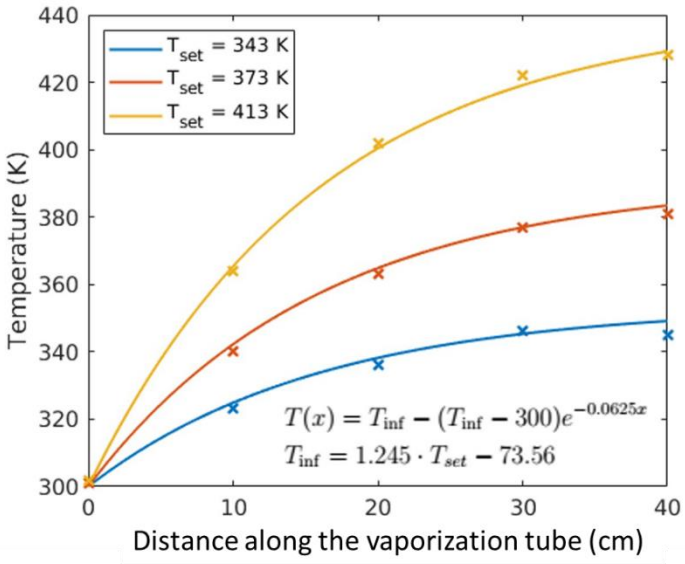

Figure S1. Monitored (markers) and fitted (solid lines, using the equation given in the figure) temperature profile within the VIA vaporization tube. The measurements used the same dataset as the one in Fig. 3b.

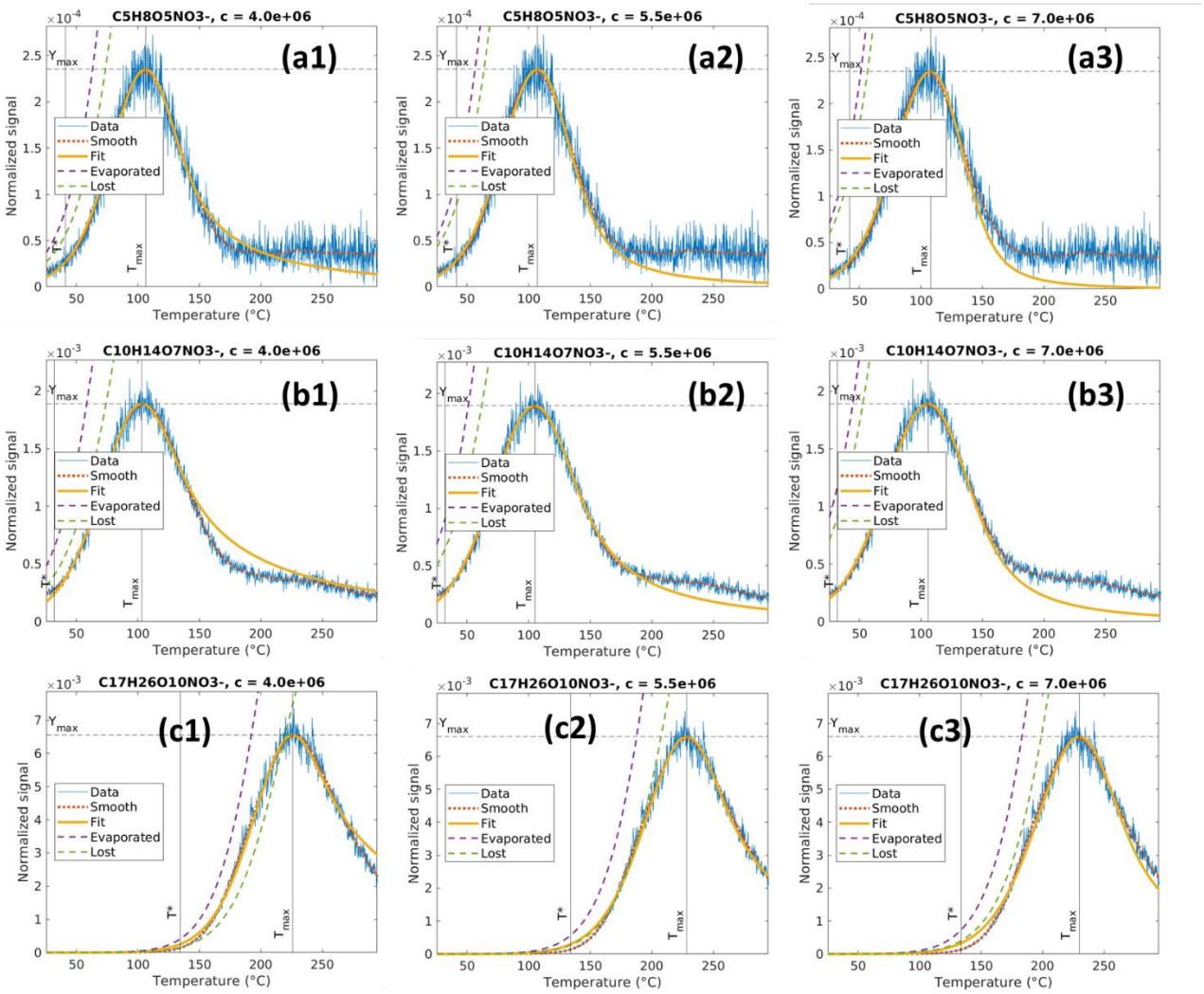

Figure S2. Examples for the determination of the proportionality constant c used in Eq. (3) for (a1-a3) $C_5H_8O_5$, (b1-b3) $C_{10}H_{14}O_7$, and (c1-c3) $C_{17}H_{26}O_{10}$. Note that the fitting results are not very sensitive to this constant (except tails of the thermograms) and a value of 5.5e6 was used in the model.

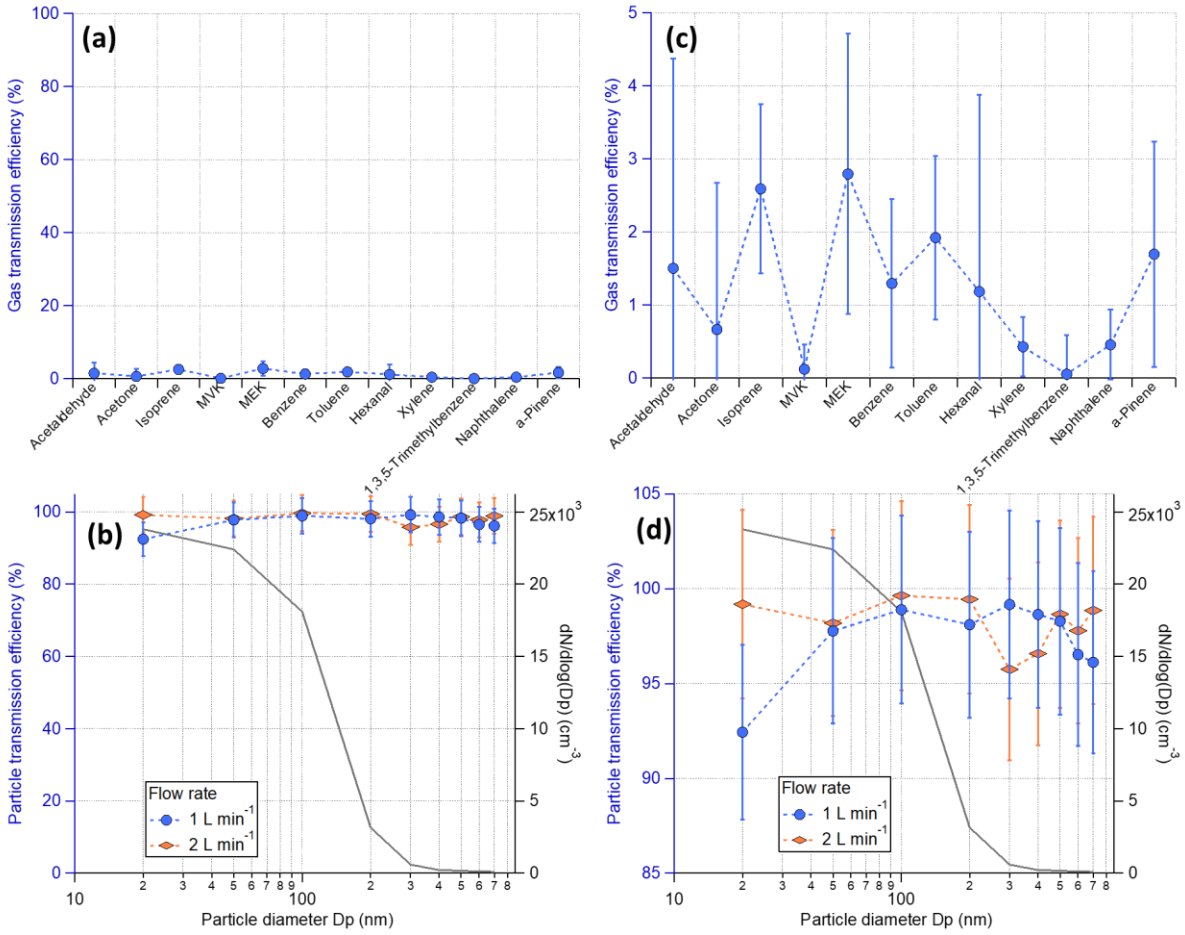

Figure S3. Transmission efficiency of (a) volatile organic compounds (we used 1 L min^{-1} for this test because it is the sampling flow for the PTR-TOF) and (b) monodispersed 20-700 nm ammonium sulfate (AS) particles (measured by a CPC) through the gas denuder. Panels (c) and (d) used the same datasets as panel (a) and (b), respectively, but zoom in to show the details. The reference size distribution of the tested AS particles is shown as grey lines in panel (b) and (d).

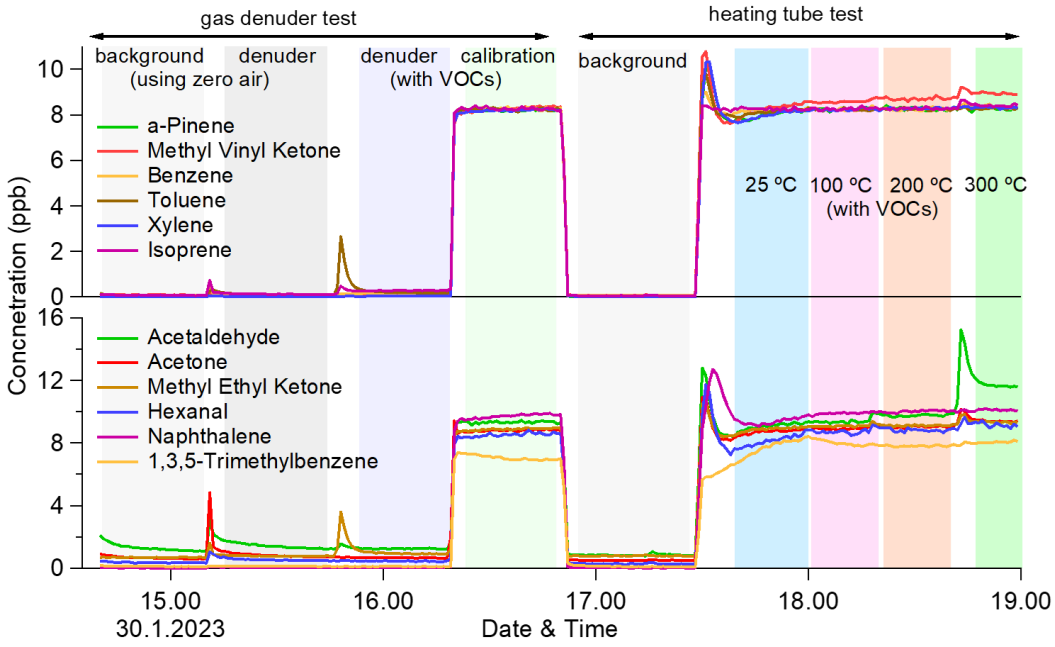

Figure S4. Evaluation of the gas removal efficiency of the gas denuder and the gas transmission efficiency of the vaporization (heating) tube during the PTR-TOF calibration. The increase of some VOC species at the highest temperature during the vaporization tube test was owing to the evaporation of gas, condensed during the low temperature stages, from the tubing wall.

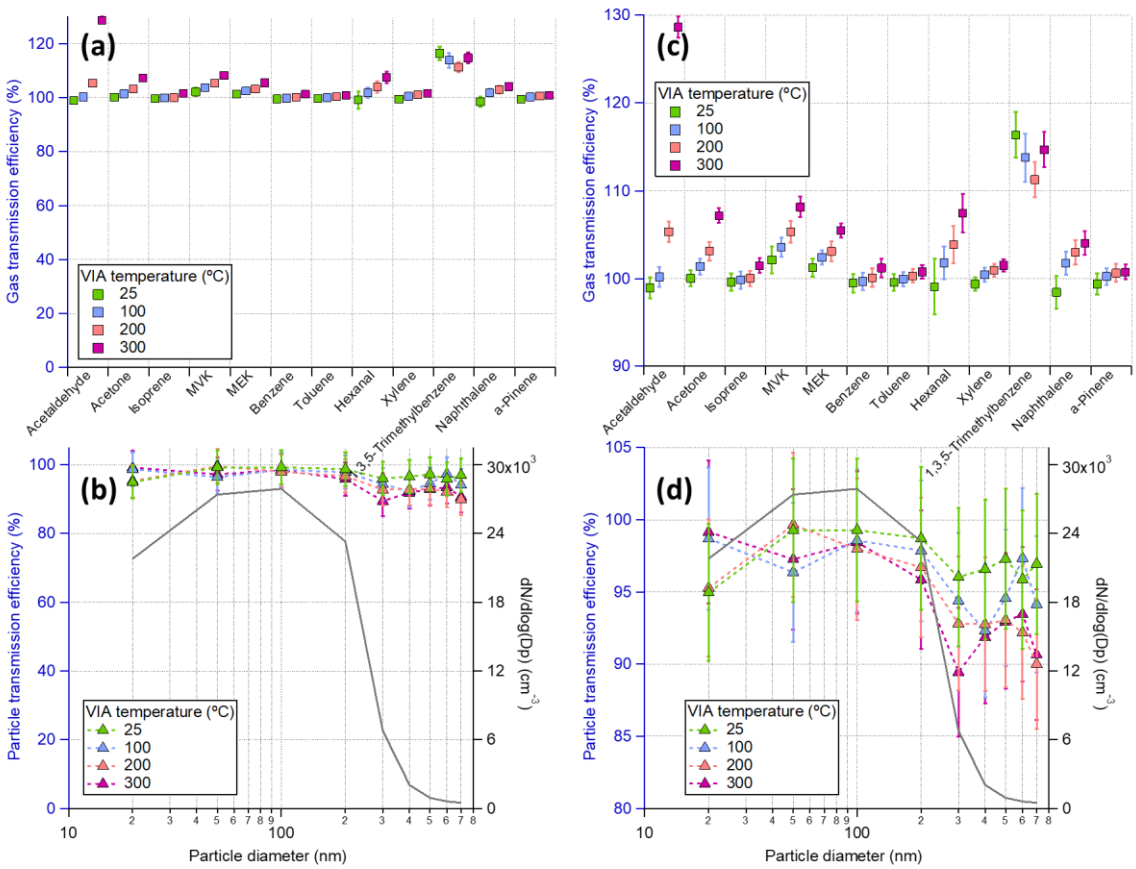

Figure S5. Transmission efficiency of (a) gas compounds (measured by a PTR-TOF) and (b) monodispersed 20-700 nm NaCl particles (measured by a CPC) within the VIA vaporization tube at four different temperatures (25, 100, 200, and 300 °C) with a flow rate of 1 L min^{-1}. Panels (c) and (d) used the same datasets as panel (a) and (b), respectively, but zoom in to show the details. The reference size distribution of the tested AS particles is shown as grey lines in panel (b) and (d).

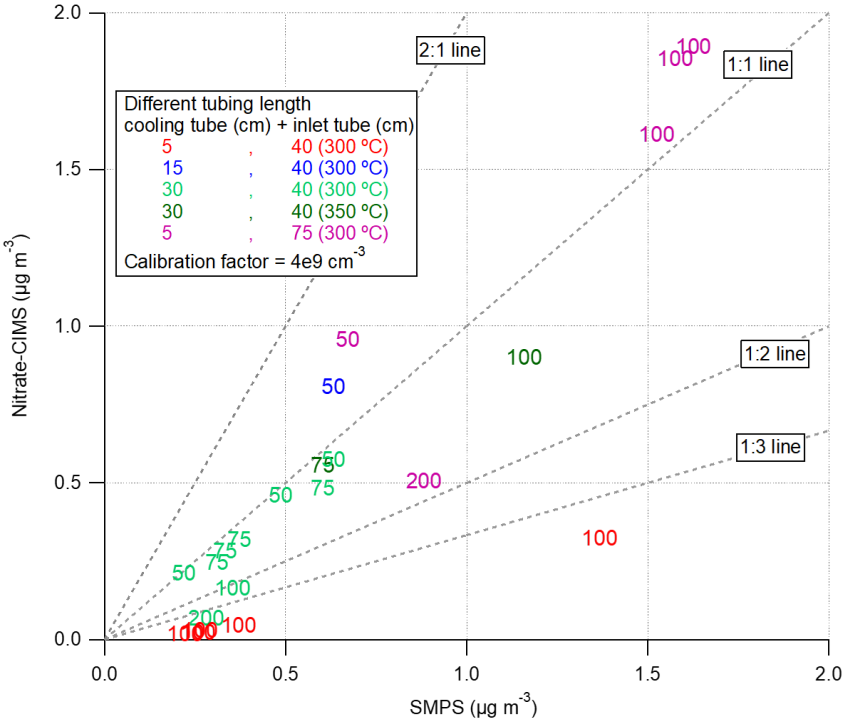

Figure S6. Comparison between the sulfuric acid concentrations measured by the NO_3-CIMS vs. the evaporated sulfuric acid mass estimated from the SMPS measurements. Different colors represent different setups used for this comparison and the number of each marker shows the size of ammonium sulfate particles (nm) selected.

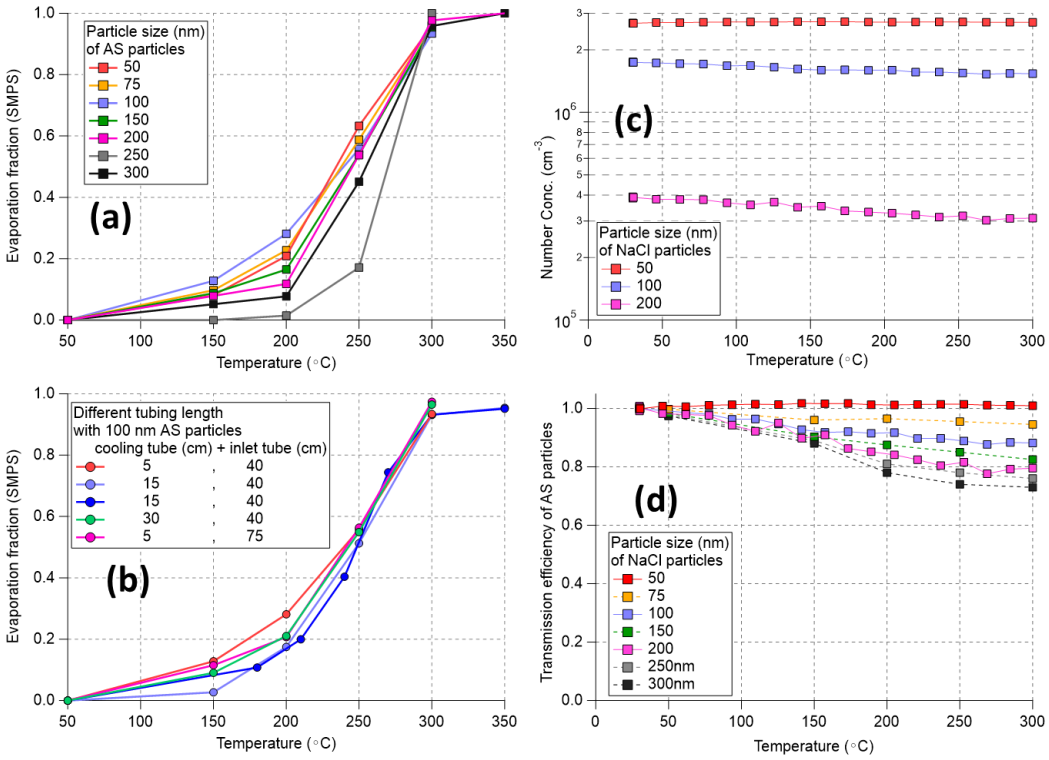

Figure S7. Evaluation of the evaporation efficiency of the vaporization tube for (a) size-selected (50-200 nm) ammonium sulfate (AS) particles with fixed setup (i.e. 5 cm cooling tube and 40 cm inlet), and (b) different setup with 100 nm ammonium sulfate particles. A cooling tube is used between the VIA vaporization tube and the sheath flow unit to cool down the hot sampling flow before it mixes with the sheath flow to decrease potential turbulence within (and after) the sheath flow piece. (c) Number concentration and (d) transmission efficiency of size-selected sodium chloride (NaCl) particles as a function of VIA temperature. Lower transmissions at higher temperatures would be misinterpreted as evaporation if not being considered, thus overestimate the evaporation efficiency. In panel (d), the particle transmission efficiency was evaluated for the entire VIA inlet system. The transmission efficiency of 75 and 150 nm AS particles were interpolated and the transmission efficiency of 75 and 150 nm AS particles (dashed lines and markers) were extrapolated using the measurements at the other three sizes (solid line and markers).

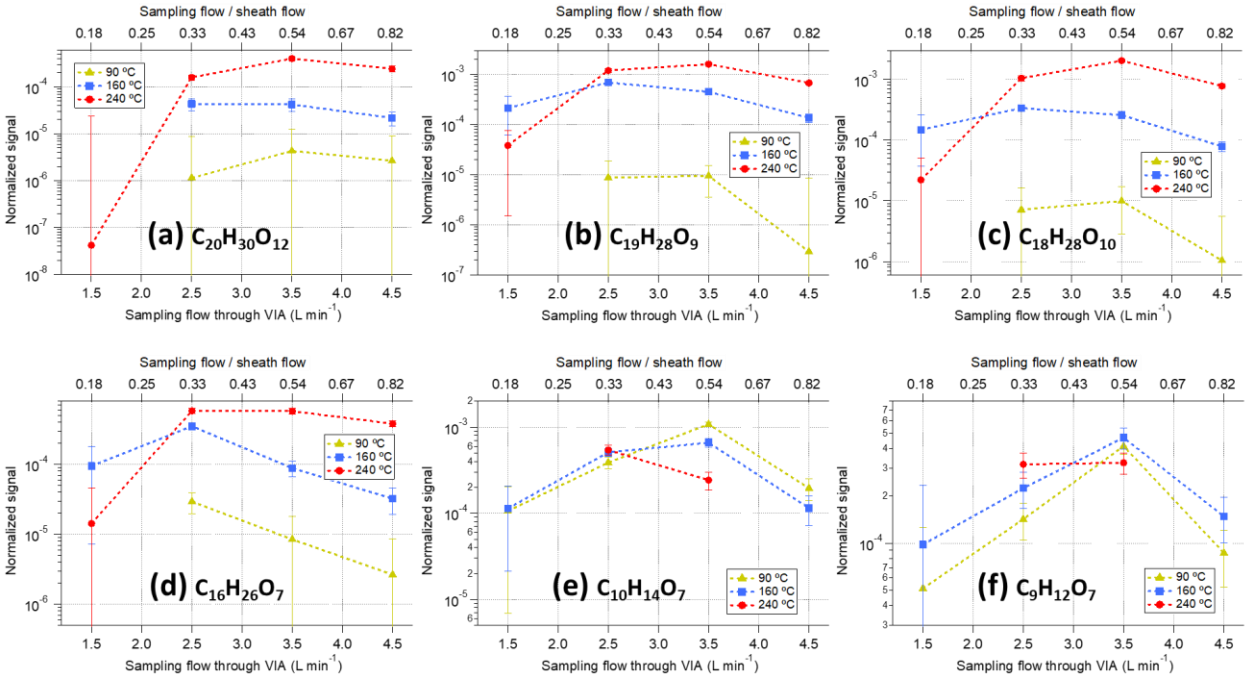

Figure S8. The effects of different sampling flow rates on the sensitivity of HOM species with a stable SOA (14 ± 1.5 µg m^{-3}) input at three different temperatures. HOM signals were normalized to the reagent ions. The dilution factors of different flow ratios were applied for HOM signals for straight forward comparisons.

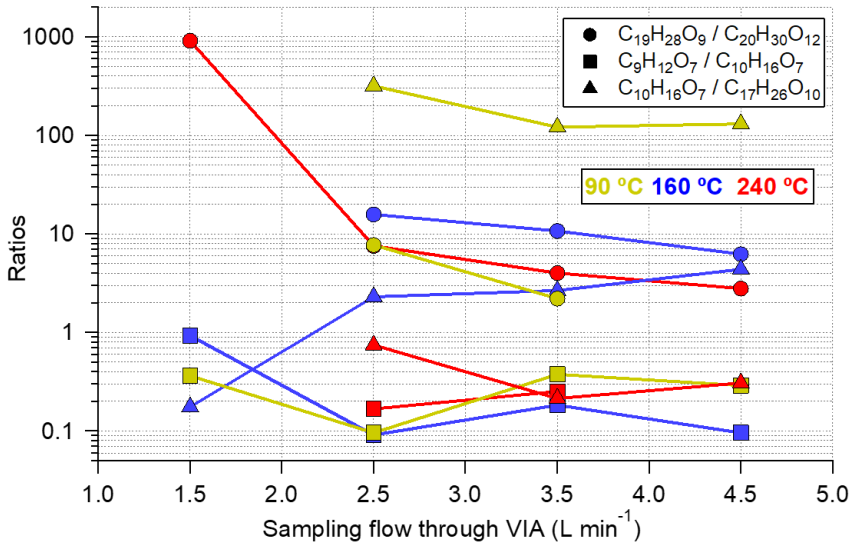

Figure S9. Relative changing between HOM species (circle: two different dimers, square: two different monomers, and triangle: one monomer and one dimer) as a function of sampling flow rate.

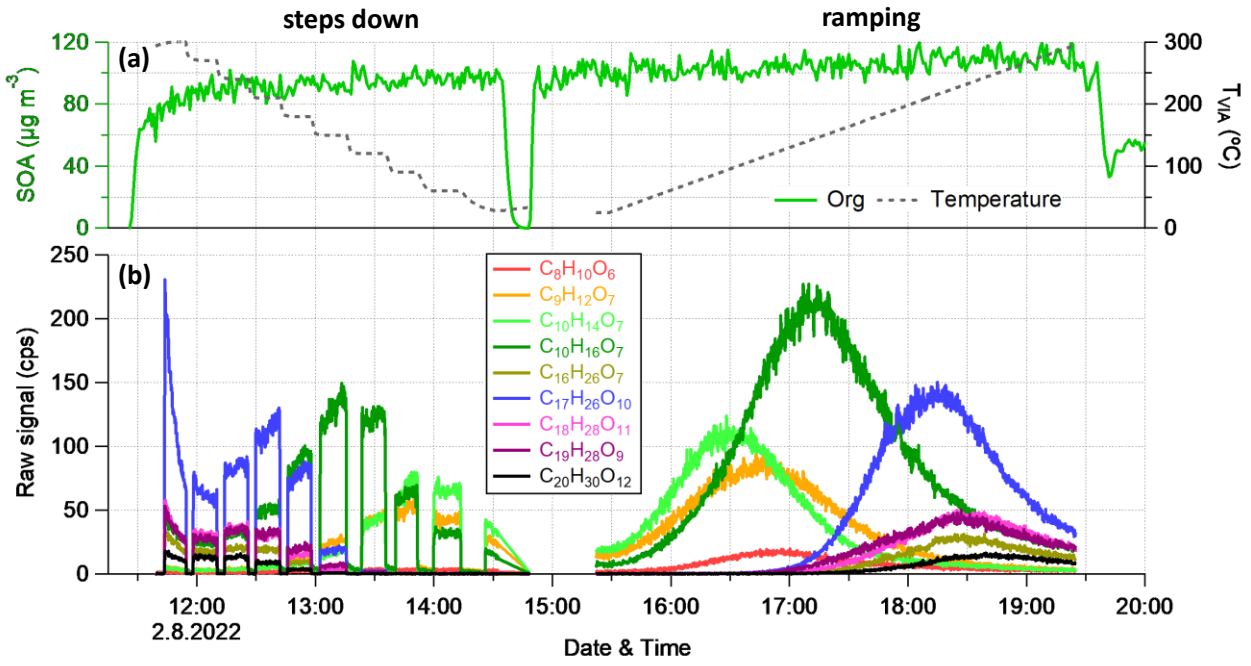

Figure S10. Comparisons between the "steps" and "ramping" modes for (a) SOA measured by the AMS (1.5 min) and temperature of the VIA vaporization tube monitored by a thermocouple, and (b) HOM species (10-s data set). Note that the measurement of steps mode was very unstable during the start of the experiments (VIA heated at 300 ºC), which was suspected to be affected by contaminations from the previous experiment.

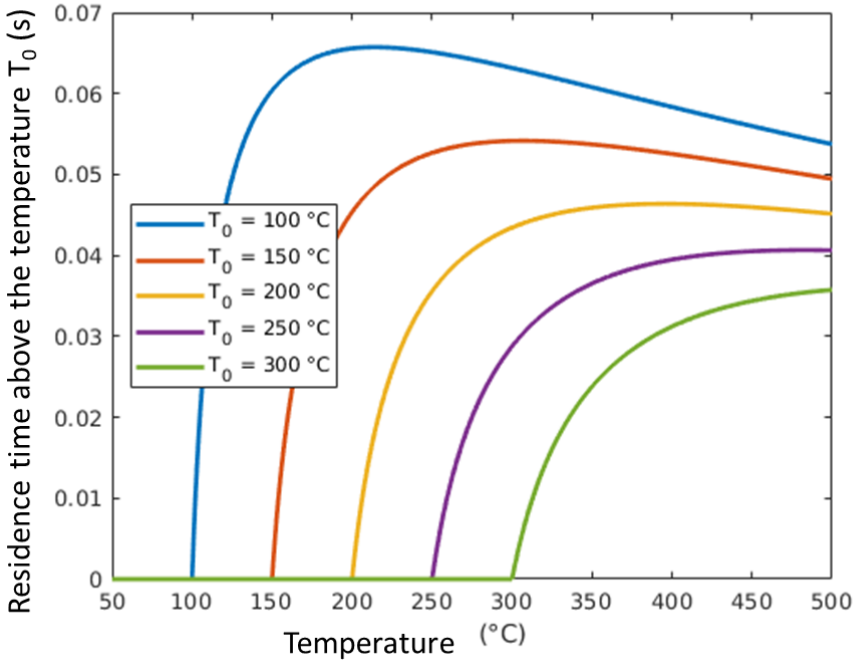

Figure S11. Residence time above the temperature T_0 as a function of the VIA set temperature.

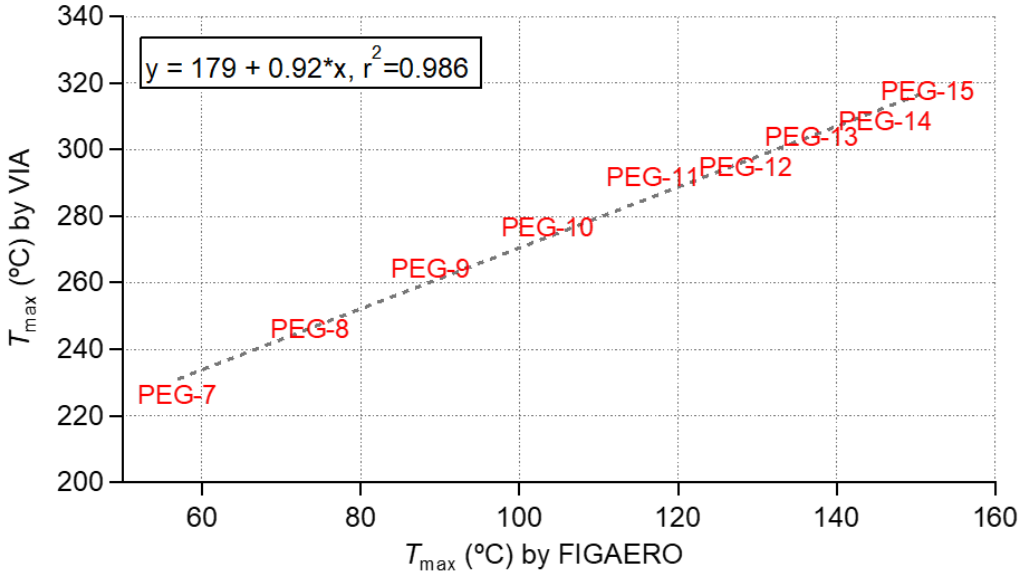

Figure S12. Comparison of T_{max} measured for the homogenous series of PEGs using the VIA-NO_3-CIMS and FIGAERO-iodide-CIMS systems. The T_{max} for PEGs obtained from the VIA-NO_3-CIMS system are summarized in Table S4.

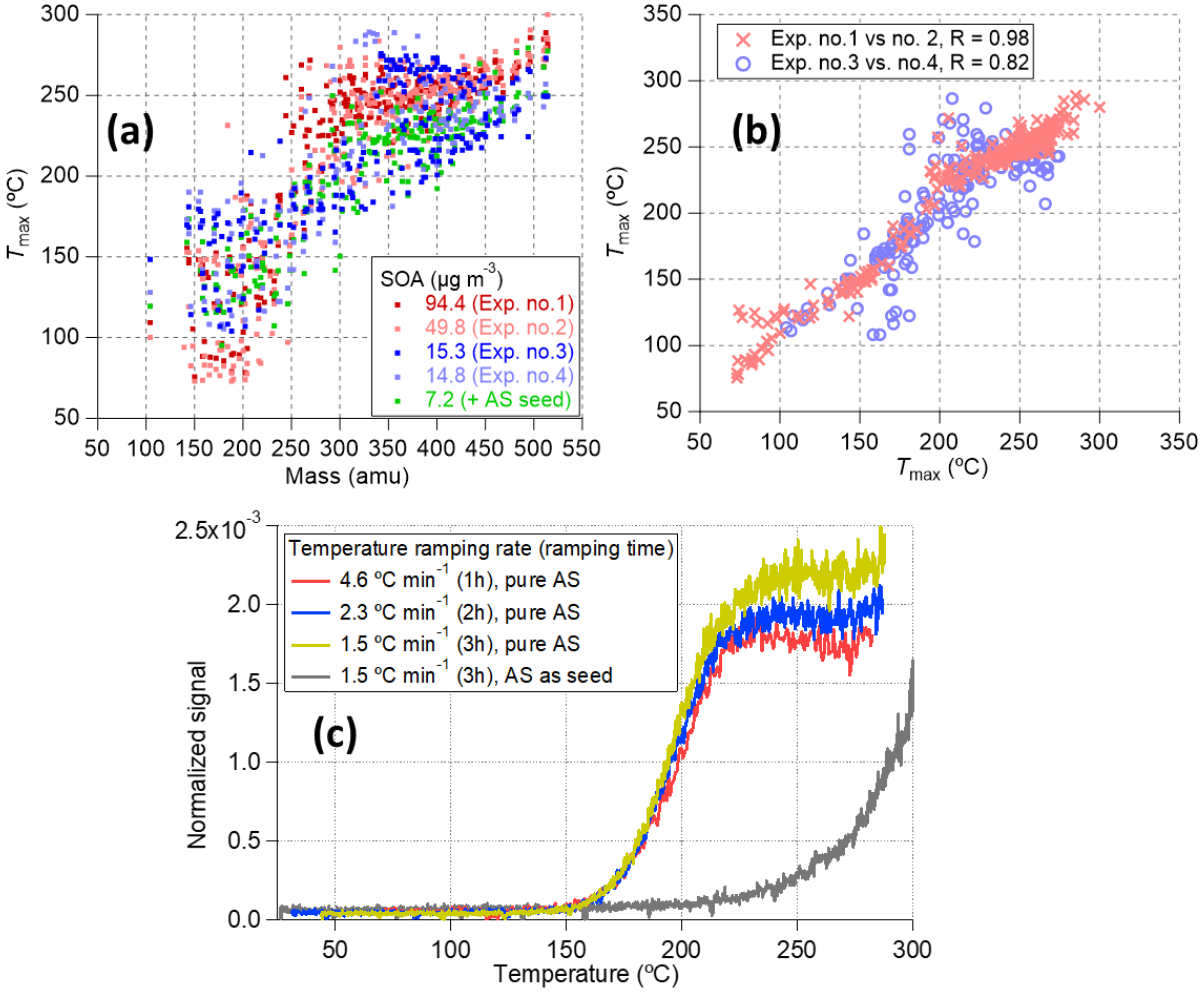

130

Figure S13. (a) The VIA datasets used to make the mean and the standard deviation of T_{max} in Figure 7a. (b) Comparisons of T_{max} obtained from different experiments. (C) Thermogram of sulfuric acid evaporated from 100-nm ammonium sulfate (AS) particles in different experiments.

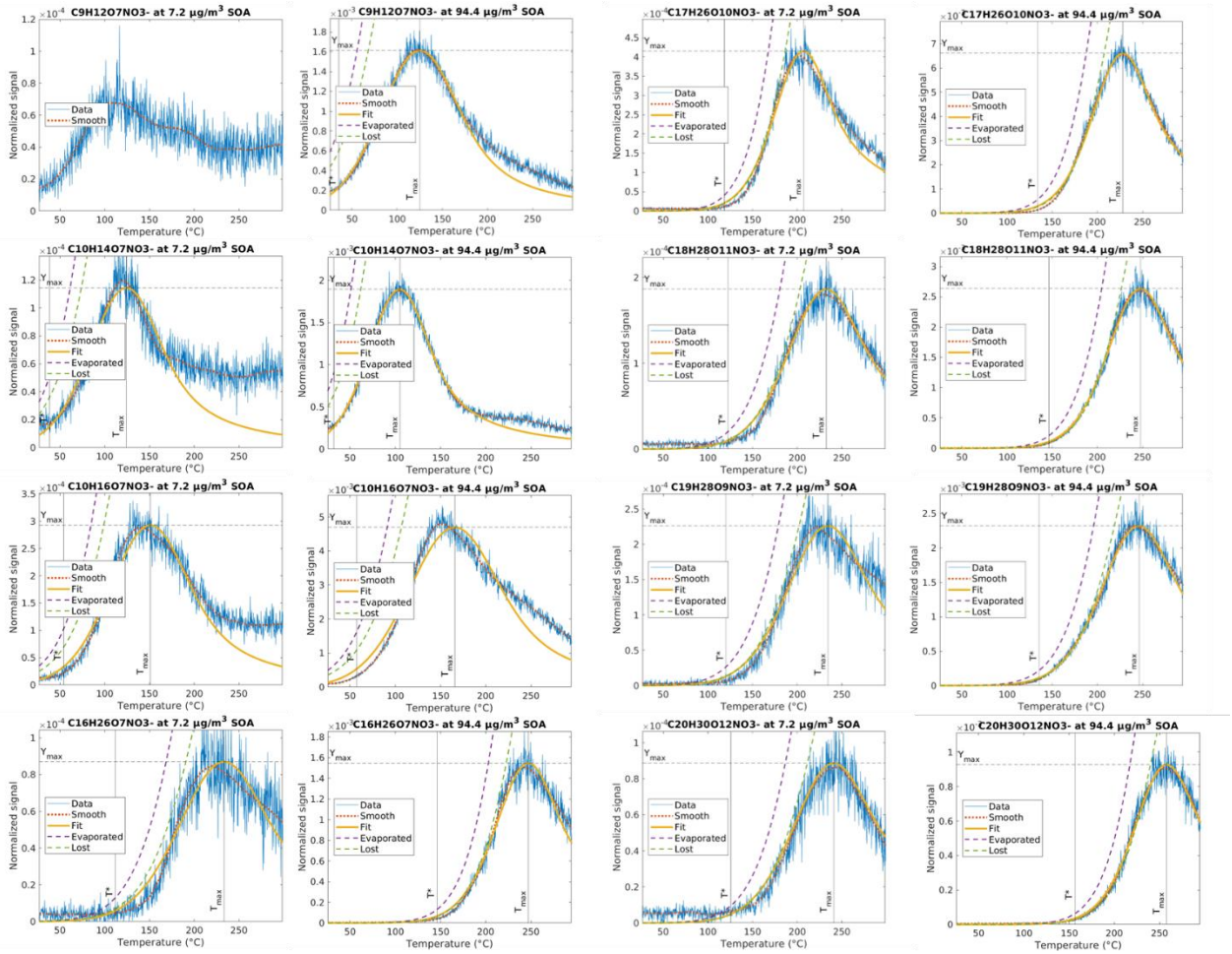

135

Figure S14. More examples of the fitting results compared to the measured thermograms of different HOM species.

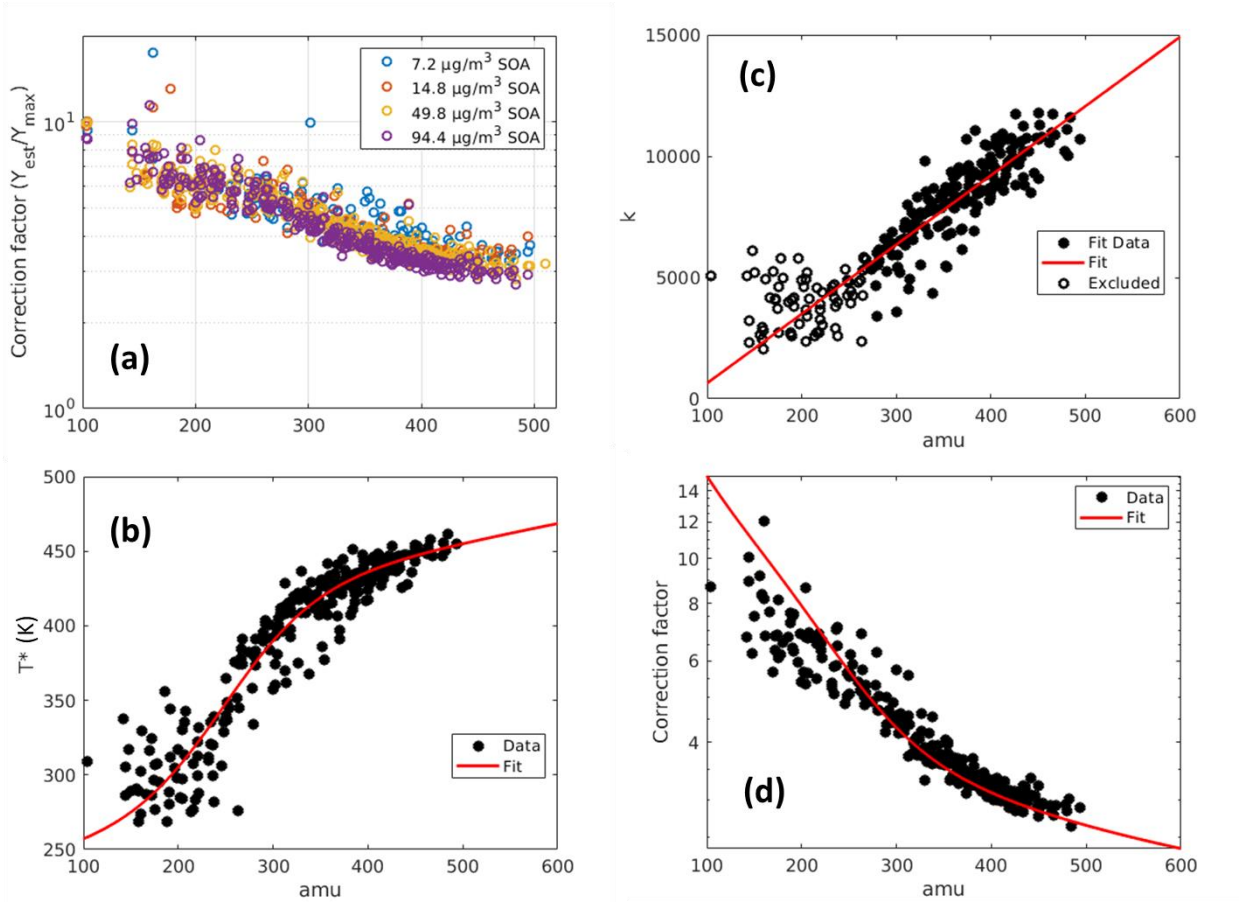

Figure S15. (a) The same plot as Fig. 8b but in log scale. The fitted parameter (b) *k* and (c) T^*, and (d) the correction factor as a function of molecular mass for the 94.4 µg m^{-3} SOA dataset. In panel (c), species with masses lower than 300 amu did not show any trend with mass and were therefore not included in the fit. (d) The estimated correction factor based on only atomic mass, utilizing the fits from panels (b) and (c). For low-molecular-mass species the fit is not as good due to the fits in panels (b) and (c) not describing these species very well. Similar fits were made for all datasets in to obtain the curves displayed in panel (a) and Figure 8b.

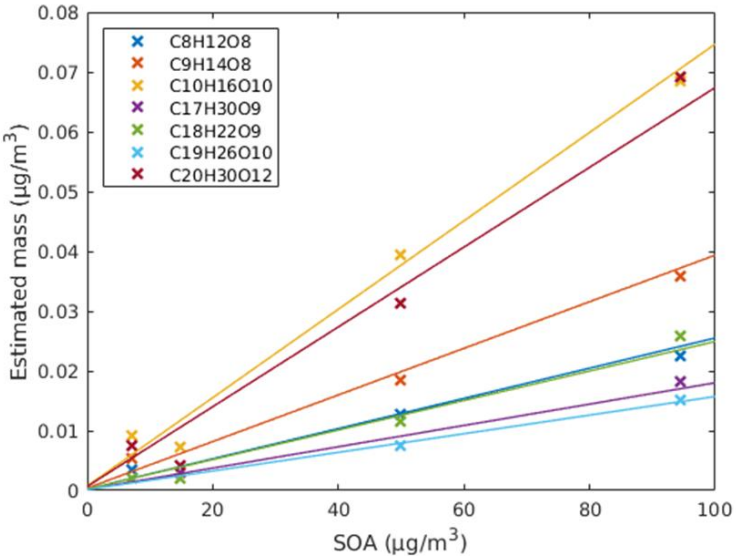

Figure S16. Estimated mass concentrations of HOM species vs. SOA. Some data points were missing because of relatively messy thermograms.

Table S1. (Semi-) Online techniques for the measurements of particle-phase organic compounds.

Instrument	Time resolution	Desorption temperature (°C)	Ionization method	Particle size (nm)	[b]Detection limit (ng m^{-3})	Reference
[1]TDCIMS	~10-20 min	300	H_3O^+, O_2^-, CO_3^-	6-20	~0.05	(Voisin et al., 2003; Smith et al., 2004)
[2]Aerosol-CIMS	1 s	480	$(H_2O)_nH^+$, NO^+, F^-, O_2^+, SF_6^-…	[a]/	100-200	(Hearn and Smith, 2004; Hearn and Smith, 2006)
[3]TAG GC/MS-FID	1 hour	30-300	electron impact	> 60	0.1-23	(Williams et al., 2006)
[4]MOVI-CIMS	10-90 min	40-150	CH_3COO^-, H_3O^+, I^-, SF_6^-	> 130	0.8-2.6	(Yatavelli and Thornton, 2010; Yatavelli et al., 2012)
[5]FIGAERO-CIMS	20-45 min	25-200	CH_3COO^-, I^-	/	0.01-1.7	(Lopez-Hilfiker et al., 2014)
[6]CHARO-PTR	seconds	50-250	H_3O^+	100-750	10-20	(Eichler et al., 2015)
[7]EESI-TOF	1 s	< 250	Na^+	/	1-10	(Lopez-Hilfiker et al., 2019)
[8]TD-PTR-ITMS	30 min	150	H_3O^+	> 450	12	(Thornberry et al., 2009)
[9]TD-PTR-MS	~45 min	25-350	H_3O^+	70-2000	0.2	(Holzinger et al., 2010)
[10]AeroFAPA-MS	seconds	< 150	H_3O^+, O_2^+, NO^+, O^-…	/	~7	(Brüggemann et al., 2015)
VIA-NO_3-CIMS	1 s	25-350	NO_3^-	/	~1	(Häkkinen et al., 2023)

Notes:
[1]TDCIMS: Thermal Desorption Chemical Ionization Mass Spectrometer
[2]Aerosol-CIMS: Aerosol Chemical Ionization Mass Spectrometer
[3]TAG-GCMS/FID: Thermal Desorption Aerosol Chromatography Mass Spectrometer and Flame Ionization Detector
[4]MOVI-CIMS: Micro Orifice Volatilization Impactor Chemical Ionization Mass Spectrometer
[5]FIGAERO-CIMS: Filter Inlet for Gases and AEROsols Chemical Ionization Mass Spectrometer
[6]CHARO-PTR:
[7]EESI-TOF: Extractive ElectroSpray Ionization Time-Of-Flight mass spectrometer
[8]TD-PTR-ITMS: Collection/Thermal-Desorption Proton-Transfer-Reaction Ion Trap Mass Spectrometer
[9]TD-PTR-MS: Thermal-Desorption Proton-Transfer-Reaction Mass Spectrometer
[10]AeroFAPA-MS: Aerosol Flowing Atmospheric-Pressure Afterglow Mass Spectrometry
[a]/: means that this technique is not selective to some specific size range, thus an external device (e.g. a cyclone or a differential mobility analyzer) can be used to chosen the size(s) of interest.
[b]Detection limit: calculated as three times the standard deviation during background/blank measurements.

Table S2. Muti-component calibration mixture in nitrogen used in this study.

Compound	Formula	Molecular mass (g mol^{-1})	CAS#	Uncertainty
Acetaldehyde	C_2H_4O	44.05	75-07-0	± 5%
Acetone	C_3H_6O	58.08	67-64-1	± 5%
Isoprene	C_5H_8	68.12	78-79-5	± 5%
Methyl Vinyl Ketone	C_4H_6O	70.09	78-94-4	± 5%
Methyl Ethyl Ketone	C_4H_8O	72.11	78-93-3	± 5%
Benzene	C_6H_6	78.11	71-43-2	± 5%
Toluene	C_7H_8	92.14	108-88-3	± 5%
Hexanal	$C_6H_{12}O$	100.16	66-25-1	± 5%
m-Xylene	C_8H_{10}	106.17	108-38-3	± 5%
p-Xylene	C_8H_{10}	106.17	106-42-3	± 5%
1,3,5-Trimethylbenzene	C_9H_{12}	120.20	108-67-8	± 5%
Naphthalene	$C_{10}H_8$	128.17	91-20-3	± 5%
α-Pinene	$C_{10}H_{16}$	136.23	80-56-8	± 5%

Table S3. Chemicals that were atomized to generate aerosol particles used in this study.

Compound	Formula	Molecular mass (g mol^{-1})	CAS#	Purity
[1]Ammonium nitrate	NH_4NO_3	80.04	6484-52-2	> 99%
Ammonium sulfate	$(NH_4)_2SO_4$	132.14	7783-20-2	> 99%
Sodium chloride	NaCl	58.44	7647-14-5	> 99%
[2]PEG-6 (Hexaethylene glycol)	$C_{12}H_{26}O_7$	282.33	2615-15-8	> 97%
PEG 400	$C_{2n}H_{4n+2}O_{n+1}$	380-420	25322-68-3	mixture

Notes:

[1]Ammonium nitrate was only used for the ionization efficiency calibration of the AMS.

[2]PEG: a homologous series of polyethylene glycol, has molecular formula as $H{-}(O{-}CH_2{-}CH_2)_n{-}OH$. In this study, we used pure PEG-6 (i.e. n=6) and a mixture of oligomers PEG 400 (with average n =8.2 to 9.1) for the experiments.

Table S4. Summary of all PEG peaks identified from the PEG 400 solution using the VIA-NO_3-CIMS system.

Compound	Formula	m/z (with NO_3^-)	T_{max} (°C)
PEG-6	$C_{12}H_{26}O_7$	344	/
PEG-7	$C_{14}H_{30}O_8$	388	226.1
PEG-8	$C_{16}H_{34}O_9$	432	246.1
PEG-9	$C_{18}H_{38}O_{10}$	476	264.2
PEG-10	$C_{20}H_{42}O_{11}$	520	276.4
PEG-11	$C_{22}H_{46}O_{12}$	564	291.6
PEG-12	$C_{24}H_{50}O_{13}$	608	294.6
PEG-13	$C_{26}H_{54}O_{14}$	652	303.8
PEG-14	$C_{28}H_{58}O_{15}$	696	308.4
PEG-15	$C_{30}H_{62}O_{16}$	740	317.5
PEG-16	$C_{32}H_{66}O_{17}$	784	323.6

Table S5. The cells correspond to the correction factors for the plots in Figure S2.

Compound	c		
	4e6	5.5e6	7e6
$C_5H_8O_5$	4.48	6.30	8.25
$C_{10}H_{14}O_7$	3.52	4.89	6.37
$C_{17}H_{26}O_{10}$	2.41	3.16	3.97

Reference

Brüggemann, M., Karu, E., Stelzer, T., and Hoffmann, T.: Real-Time Analysis of Ambient Organic Aerosols Using Aerosol Flowing Atmospheric-Pressure Afterglow Mass Spectrometry (AeroFAPA-MS), Environ. Sci. Technol., 49, 5571-5578, 10.1021/es506186c, 2015.

Eichler, P., Müller, M., D'Anna, B., and Wisthaler, A.: A novel inlet system for online chemical analysis of semi-volatile submicron particulate matter, Atmos. Meas. Tech., 8, 1353-1360, 10.5194/amt-8-1353-2015, 2015.

Hearn, J. D. and Smith, G. D.: A chemical ionization mass spectrometry method for the online analysis of organic aerosols, Anal. chem., 76, 2820-2826, 10.1021/ac049948s, 2004.

Hearn, J. D. and Smith, G. D.: Reactions and mass spectra of complex particles using Aerosol CIMS, Int. J. Mass spectrom., 258, 95-103, 10.1016/j.ijms.2006.05.017, 2006.

Hinds, W.: Aerosol technology: Properties, behavior, and measurement of airborne particles, 1999.

Holzinger, R., Williams, J., Herrmann, F., Lelieveld, J., Donahue, N. M., and Röckmann, T.: Aerosol analysis using a Thermal-Desorption Proton-Transfer-Reaction Mass Spectrometer (TD-PTR-MS): a new approach to study processing of organic aerosols, Atmos. Chem. Phys., 10, 2257-2267, 10.5194/acp-10-2257-2010, 2010.

Häkkinen, E., Zhao, J., Graeffe, F., Fauré, N., Krechmer, J. E., Worsnop, D., Timonen, H., Ehn, M., and Kangasluoma, J.: Online measurement of highly oxygenated compounds from organic aerosol, Atmos. Meas. Tech., 16, 1705-1721, 10.5194/amt-16-1705-2023, 2023.

Lopez-Hilfiker, F. D., Pospisilova, V., Huang, W., Kalberer, M., Mohr, C., Stefenelli, G., Thornton, J. A., Baltensperger, U., Prevot, A. S. H., and Slowik, J. G.: An extractive electrospray ionization time-of-flight mass spectrometer (EESI-TOF) for online measurement of atmospheric aerosol particles, Atmos. Meas. Tech., 12, 4867-4886, 10.5194/amt-12-4867-2019, 2019.

Lopez-Hilfiker, F. D., Mohr, C., Ehn, M., Rubach, F., Kleist, E., Wildt, J., Mentel, T. F., Lutz, A., Hallquist, M., Worsnop, D., and Thornton, J. A.: A novel method for online analysis of gas and particle composition: description and evaluation of a Filter Inlet for Gases and AEROsols (FIGAERO), Atmos. Meas. Tech., 7, 983-1001, 10.5194/amt-7-983-2014, 2014.

Schobesberger, S., amp, apos, Ambro, E. L., Lopez-Hilfiker, F. D., Mohr, C., and Thornton, J. A.: A model framework to retrieve thermodynamic and kinetic properties of organic aerosol from composition-resolved thermal desorption measurements, Atmos. Chem. Phys., 18, 14757-14785, 10.5194/acp-18-14757-2018, 2018.

Smith, J. N., Moore, K. F., McMurry, P. H., and Eisele, F. L.: Atmospheric measurements of sub-20 nm diameter particle chemical composition by thermal desorption chemical ionization mass spectrometry, Aerosol Sci. Technol., 38, 100-110, 10.1080/02786820490249036, 2004.

Thornberry, T., Murphy, D. M., Thomson, D. S., de Gouw, J., Warneke, C., Bates, T. S., Quinn, P. K., and Coffman, D.: Measurement of Aerosol Organic Compounds Using a Novel Collection/Thermal-Desorption PTR-ITMS Instrument, Aerosol Sci. Technol., 43, 486-501, 10.1080/02786820902763132, 2009.

Voisin, D., Smith, J. N., Sakurai, H., McMurry, P. H., and Eisele, F. L.: Thermal Desorption Chemical Ionization Mass Spectrometer for Ultrafine Particle Chemical Composition, Aerosol Sci. Technol., 37, 471-475, 10.1080/02786820300959, 2003.

Williams, B. J., Goldstein, A. H., Kreisberg, N. M., and Hering, S. V.: An In-Situ Instrument for Speciated Organic Composition of Atmospheric Aerosols:Thermal DesorptionAerosolGC/MS-FID (TAG), Aerosol Sci. Technol., 40, 627-638, 10.1080/02786820600754631, 2006.

Yatavelli, R. L. N. and Thornton, J. A.: Particulate Organic Matter Detection Using a Micro-Orifice Volatilization Impactor Coupled to a Chemical Ionization Mass Spectrometer (MOVI-CIMS), Aerosol Sci. Technol., 44, 61-74, 10.1080/02786820903380233, 2010.

Yatavelli, R. L. N., Lopez-Hilfiker, F., Wargo, J. D., Kimmel, J. R., Cubison, M. J., Bertram, T. H., Jimenez, J. L., Gonin, M., Worsnop, D. R., and Thornton, J. A.: A Chemical Ionization High-Resolution Time-of-Flight Mass Spectrometer Coupled to a Micro Orifice Volatilization Impactor (MOVI-HRToF-CIMS) for Analysis of Gas and Particle-Phase Organic Species, Aerosol Sci. Technol., 46, 1313-1327, 10.1080/02786826.2012.712236, 2012.